Linear Perturbation Amplification in Self-Similar Ablation Flows of Inertial Confinement Fusion

F. Abéguilé,* C. Boudesocque-Dubois, J.-M. Clarisse,† S. Gauthier, and Y. Saillard

CEA/Bruyères-Le-Châtel, Boîte Postale 12, 91680 Bruyères-Le-Châtel, France

(Received 21 July 2005; published 21 July 2006)

Exact similarity solutions for inviscid compressible ablative flows in slab symmetry with nonlinear heat conduction are proposed for studying unsteadiness and compressibility effects on the hydrodynamic stability of ablation fronts relevant to inertial confinement fusion. Both the similarity solutions and their linear perturbations are numerically computed with a dynamical multidomain Chebyshev pseudospectral method. Herewith the first analysis of laser-imprinting based on a dynamic solution is presented, showing that maximum perturbation amplification occurs for a laser-intensity modulation of zero transverse wave number, with growth dominated by the mean flow stretching.

DOI: 10.1103/PhysRevLett.97.035002 PACS numbers: 52.57.−z, 47.20.−k, 52.35.Py, 52.38.Mf

Hydrodynamic instabilities are a key issue in laser-driven inertial confinement fusion (ICF) where thermonuclear burn is expected to be achieved for a sufficiently symmetric implosion of a spherical capsule [1]. Implosions of such capsules are highly nonuniform and unsteady complex flows, hence rendering their stability analysis particularly arduous. Most of the theoretical work devoted to ICF target hydrodynamic stability has dealt with the so-called ''ablative Rayleigh-Taylor (RT)'' instability [2] which occurs during the shell acceleration phase [1]. Numerous analytical models, established for idealized ablation flows—i.e., considering a steady ablative flow of an unbounded domain in a uniform and constant inertial force field, continuous or discontinuous ablation profiles, as well as other, more or less restrictive assumptions (e.g., incompressible or isobaric approximations)—have been proposed for this instability linear regime [3]. These models have undoubtedly contributed to a better understanding of this rather complex instability in the case of steady ablation fronts. Certain key features of ICF implosions—such as mean flow unsteadiness, nonuniformities, compressibility, convergence—cannot however be properly rendered by such analytical models. Overcoming such limitations is generally thought of as being a matter of multidimensional numerical simulations of perturbed ablation flows using ''full-physics'' hydrodynamics codes. Here we propose a different approach by considering the linear stability of exact one-dimensional (1D) self-similar ablation flows in the deflagration regime [4–11]. These similarity solutions are especially relevant to the early stage of capsule irradiation—the so-called ''shock-transit time''—for which numerical simulations indicate that mean flow profiles, even for constant irradiation fluxes, are more akin to self-similar than to steady solutions [12]. Perturbed ablation-front evolutions need to be accurately described during this phase which is critical to ICF target implosions since it sets initial conditions for the subsequent ablative RT growth. For unsteady mean flows, achieving this goal without impairing the validity of the results requires a numerical approach. Here, the rigorous framework of the mean flow similarity allows us to use highly accurate numerical methods [13]—namely dynamical multidomain Chebyshev spectral methods—for computing both the mean flow and its 3D perturbations, hence avoiding the flaws of overly dissipative and dispersive numerical schemes found in ICF hydrocodes. We are thus able to produce, with unprecedented details and accuracy, linear perturbation responses for ablation flows relevant to ICF, while taking into account—without any restriction, yet within a simplified setting—unsteadiness, compressibility, and small-scale nonlinear heat-conduction effects. In this Letter, we report on newly obtained results regarding both self-similar ablative flows and the first analysis of the laser-imprinting problem of direct-drive irradiation [12,14,15] in the case of unsteady mean flows.

Consider the 1D motion in the x direction of a compressible, inviscid, heat-conducting fluid with a polytropic equation of state $p = \rho RT$, $\mathcal{E} = C_v T$, $C_v = R/(\gamma - 1)$, and a nonlinear heat conductivity of the form

$$\kappa = \chi(\rho_0/\rho)^{\mu}(T/T_0)^{\nu}, \qquad \mu \geq 0, \qquad \nu \geq 1, \tag{1}$$

where ρ_0, T_0 are some standard density and temperature. The equations of motion, written in terms of the Lagrangian coordinate m such that $dm = \rho dx$, read

$$\begin{gathered} \partial_t(1/\bar{\rho}) - \partial_m \bar{v}_x = 0, \qquad \partial_t \bar{v}_x + \partial_m \bar{p} = 0, \\ \partial_t(\bar{v}_x^2/2 + C_v \bar{T}) + \partial_m(\bar{p}\bar{v}_x + \bar{\varphi}_x) = 0, \end{gathered} \tag{2}$$

where $\bar{\rho}$, $\bar{v}_x$, $\bar{p}$, $\bar{T}$, $\bar{\varphi}_x (= -\kappa\bar{\rho}\partial_m \bar{T})$ denote, respectively, the fluid density, x velocity, pressure, temperature, and heat flux as functions of (m, t). Since the early work of Marshak [4] similarity solutions of Eq. (2), or of their two-temperature counterparts in the case of plasmas, have been investigated either by means of simulations of particular initial and boundary value problems (IBVPs) [5,6], either through asymptotic analysis [7,10] or numerical integration [9] of similarity transformed equations. However, no complete solutions of similarity boundary value problems for Eq. (2) had been published until those of Ref. [11]. The similarity solutions considered herein arise when a semi-infinite slab ($m \geq 0$), initially such that

$$\bar{\rho}(m,0)=\rho_0, \qquad \bar{v}_x(m,0)=0, \qquad \bar{T}(m,0)=0, \quad (3)$$

is subject to the boundary conditions

$$\bar{\rho}(0,t)=p_*\left(\frac{t}{t_*}\right)^{2(\alpha-1)}, \qquad \bar{\varphi}_x(0,t)=\varphi_*\left(\frac{t}{t_*}\right)^{3(\alpha-1)}, \quad (4)$$

where p_*, φ_*, t_* are some characteristic pressure, heat flux, and time. Choosing for convenience a dimensionless formulation of Eq. (2) based on the quantities ρ_0, R, χ, t_*, similarity solutions of the IBVP (2)–(4) come as [6]

$$\begin{aligned} \bar{\rho}(m,t)&=\bar{G}(\xi), \qquad \bar{v}_x(m,t)=t^{\alpha-1}\bar{V}(\xi),\\ \bar{T}(m,t)&=t^{2(\alpha-1)}\bar{\Theta}(\xi), \qquad \bar{\varphi}_x(m,t)=t^{3(\alpha-1)}\bar{\Phi}(\xi), \end{aligned} \quad (5)$$

where the vector of unknowns $\mathbf{Y}=(\bar{G},\bar{V},\bar{\Theta},\bar{\Phi})^{\mathsf{T}}$ satisfies a system of ordinary differential equations derived by Saillard in 1983 [8],

$$\mathrm{d}_\xi \mathbf{Y}=\mathcal{F}(\xi,\mathbf{Y}), \quad (6)$$

with boundary conditions

$$\bar{G}=1, \qquad \bar{V}=0, \qquad \bar{\Theta}=0, \quad \text{as } \xi\to+\infty, \quad (7)$$

$$\bar{P}=\bar{G}\,\bar{\Theta}=\mathcal{B}_p, \qquad \bar{\Phi}=\mathcal{B}_\varphi, \quad \text{for } \xi=0, \quad (8)$$

in place of, respectively, (3) and (4), and the definitions

$$\xi=m/t^\alpha, \qquad \alpha=(2\nu-1)/(2\nu-2), \quad (9)$$

for the similarity variable and exponent. Initial and boundary conditions other than (3) and (4), are encompassed by such similarity transformations [6,10]. The constants $\mathcal{B}_p$, $\mathcal{B}_\varphi$ of Eq. (8) are dimensionless numbers built from the quantities p_*, φ_*, t_*, ρ_0, R, χ, while the components of the function $\mathcal{F}$ are [8]

$$\mathcal{F}_1=\bar{G}^2N/D, \quad \mathcal{F}_2=\alpha\xi N/D, \quad \mathcal{F}_3=-\bar{G}^{\mu-1}\bar{\Theta}^{-\nu}\bar{\Phi},$$
$$\mathcal{F}_4=[\alpha\xi\mathcal{F}_3-2(\alpha-1)\bar{\Theta}]/(\gamma-1)-\alpha\xi\bar{G}\,\bar{\Theta}N/D,$$

with $N=(\alpha-1)\bar{V}+\bar{G}\mathcal{F}_3$, $D=\alpha^2\xi^2-\bar{G}^2\bar{\Theta}$. Any solution $\mathbf{Y}$ satisfying Eqs. (7) and (8) necessarily includes the singularity $D=0$ of system (6). This singularity corresponds to an isothermal characteristic curve, say $m/t^\alpha=\xi_s$, of the (m,t) plane, which is circumvented by introducing, as part of the solution, an isothermal shock wave at $\xi=\xi_s$. Such a shock wave penetrates the cold quiescent fluid together with an infinitesimal fore-running thermal wave which, taken as a whole, may be held to be a nonisothermal shock bounding the disturbed-fluid region [4]—the sole approximation we are conceding here. Henceforth, the boundary conditions (7) are replaced by the Rankine-Hugoniot (RH) conditions, at $\xi=\xi_s$, for a nonisothermal shock wave with uniform upstream state given by (7), thus defining, along with Eq. (8), a nonlinear eigenvalue problem for system (6).

The method of solution that we have devised, a refinement of that used in [11], is quite involved [16] and consists of a finite-difference shooting procedure followed by a relaxation process coupled to an adaptive multidomain Chebyshev method [17]. In practice, nine significant digit results are commonly achieved over the domain $[0,\xi_s)$ with the exception of the boundary values at ξ_s, where accuracy drops down to 4–5 significant digits due to the error made upon replacing there the wave structure by a nonisothermal shock front. Similarity solutions for various values of the boundary value parameters $\mathcal{B}_p$, $\mathcal{B}_\varphi$, of the temperature exponent ν, and of the fluid adiabatic exponent γ have been successfully computed with this method. Variations in laser intensity, fluid density, and heat conductivity are accessible within the dimensionless formulation of Eqs. (5)–(9) through proper choices of $\mathcal{B}_p$ and $\mathcal{B}_\varphi$. As an illustration, three different examples of electron heat-conduction solutions—i.e., for $\mu=0$, $\nu=5/2$ in Eq. (1), equivalently $\alpha=4/3$ in Eq. (8)—for a monoatomic gas ($\gamma=5/3$) are shown in Fig. 1. The values of the parameters $\mathcal{B}_p$, $\mathcal{B}_\varphi$ for configurations I and II (see Table I) were deduced from a simulation of the ablation of a planar plastic foil under *Laser MégaJoule* (LMJ) direct-drive conditions, while those of flow III were chosen to yield a totally different ablation picture. In all three cases (1) the undisturbed fluid region ($\xi>\xi_s$), (2) the shock-compressed region of negligible heat flux, (3) the ablation layer with steep density, velocity, and heat-flux gradients, and (4) the conduction zone extending from the origin up to the ablation layer, are clearly seen. The main flow typical lengths are listed in Table II in terms of reduced lengths: namely, $L_{\mathrm{tot}}=t^{-\alpha}[x(\xi_s)-x(0)]$ for the whole disturbed-fluid region; $L_{\mathrm{con}}=t^{-\alpha}[x(\xi_a)-x(0)]$ with ξ_a

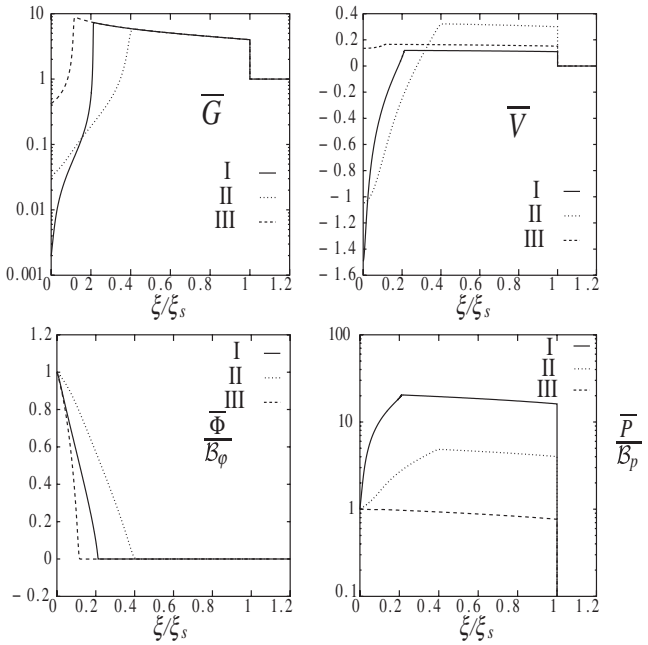

FIG. 1. Similarity solutions for $\gamma=5/3$, $\mu=0$, $\nu=5/2$. Reduced density $\bar{G}$, velocity $\bar{V}$, normalized heat flux $\bar{\Phi}/\mathcal{B}_\varphi$, and pressure $\bar{P}/\mathcal{B}_p$ profiles in the variable ξ/ξ_s (cf. Ref. [10] for a schematic view, Ref. [9] for detailed ablation layer profiles).

TABLE I. Similarity solutions of Fig. 1: parameters.

	$\mathcal{B}_p(10^{-2})$	$\mathcal{B}_\varphi(10^{-2})$	$\xi_a(10^{-1})$	$\xi_s(10^{-1})$
I	0.1	2.6	0.23	1.10
II	3.0	25.7	1.25	3.00
III	4.0	0.4	0.18	1.52

the abscissa of the flow maximum density, for the conduction zone; $L_{\rm abl} \equiv \min_\xi |\mathrm{d}_\xi \bar{G}|^{-1}$ for the ablation-front density-gradient scale length; and $L_{\rm uns}$ for the flow unstable zone according to Ref. [18]. Further characterization of these flows is provided by the ablation-front isothermal Mach number $\mathsf{M}_a = |\bar{U}_a|\bar{\Theta}_a^{-1/2}$, Froude number $\mathsf{Fr}_a = |\overline{U}_a|(|\overline{A}_a|L_{\rm abl})^{-1/2}$, and Péclet number $\mathsf{Pe}_a = \frac{\gamma}{\gamma-1} L_{\rm tot} \bar{G}_a^{1+\mu} \bar{\Theta}_a^{-\nu} |\bar{U}_a|$, where $\bar{U}_a$ and $\bar{A}_a$ are the reduced ablation velocity and front acceleration: see Table III. Froude numbers for configurations I and II are larger than unity, as is seldom during the shock-transit phase.

The linear stability of these self-similar flows is here investigated using an Eulerian description—in the (m, y, z)-coordinate system—of the flow linear perturbations, say ρ, v_x, $\mathbf{v}_\perp (= v_y \mathbf{e}_y + v_z \mathbf{e}_z)$, p, T. The relevant system of partial differential equations (PDEs) reads then

$$\partial_t \rho + \bar{\rho}(\partial_m \bar{\rho} v_x + \bar{\rho}\partial_m v_x + \partial_m \bar{v}_x \rho + \nabla_\perp \cdot \mathbf{v}_\perp) = 0,$$
$$\partial_t v_x + \bar{\rho}\partial_m \bar{v}_x v_x + \partial_m p - \partial_m \bar{p}\rho/\bar{\rho} = 0,$$
$$\partial_t \mathbf{v}_\perp + \nabla_\perp p/\overline{\rho} = \mathbf{0},$$
$$C_v(\partial_t T + \bar{\rho}\partial_m \bar{T} v_x) + \bar{\rho}\partial_m \bar{v}_x T + \bar{p}\partial_m v_x + \partial_m \varphi_x$$
$$- \partial_m \bar{\varphi}_x \rho/\bar{\rho} + (\bar{p}\nabla_\perp \cdot \mathbf{v}_\perp + \nabla_\perp \cdot \boldsymbol{\varphi}_\perp)/\bar{\rho} = 0,$$

where $\nabla_\perp . = (\partial_{y.}, \partial_{z.})^{\mathsf{T}}$. As is usual, the above 3D system of PDEs in physical space is replaced by a 1D system in the yz-Fourier space. Applying the dimensionless formulation of Eqs. (5)–(9), this system, written in the similarity variable ξ, is of the form

$$[\partial_t + \mathbf{A}(\xi, t)\partial_\xi^2 + \mathbf{B}(\xi, t)\partial_\xi + \mathbf{C}(\xi, t; k_\perp)]\mathbf{V} = \mathbf{0}, \quad (10)$$

with $\mathbf{V} = (G, V_x, \nabla_\perp \cdot \mathbf{V}_\perp, \Theta)^{\mathsf{T}}$ the yz-Fourier transform of the perturbation vector $(\rho, v_x, \nabla_\perp \cdot \mathbf{v}_\perp, T)^{\mathsf{T}}$; $k_\perp$ the transverse wave vector modulus; and where $\mathbf{A}$, $\mathbf{B}$, $\mathbf{C}$ are 4×4 matrices. Boundary conditions are provided at $\xi = 0$ by imposing arbitrary time-dependent density and incident heat-flux perturbations, and at $\xi = \xi_s$ by the nonisothermal RH conditions for linear perturbations. System (10),

TABLE II. Similarity solutions of Fig. 1: flow typical reduced lengths.

	$L_{\rm tot}$	$L_{\rm con}$	$L_{\rm abl}(10^{-3})$	$L_{\rm uns}(10^{-3})$
I	1.23	1.21	0.04	0.02
II	1.08	1.05	1.80	0.82
III	0.05	0.02	0.18	7.83

TABLE III. Similarity solutions of Fig. 1: ablation-front characteristic numbers.

	$\mathsf{M}_a(10^{-1})$	Fr_a	$\mathsf{Pe}_a(10^4)$
I	0.8	3.27	23.7
II	1.82	1.97	0.46
III	0.41	0.86	0.21

being incompletely parabolic, is handled via an operator decomposition between a reduced hyperbolic system [19] and a parabolic scalar equation, along with a proper formulation of boundary conditions for each subsystem [13]. Numerical approximation in the ξ variable is performed with the adaptive spectral method already used for the mean flow while time marching is carried out with a three-step Runge-Kutta scheme. Arbitrary perturbed configurations are amenable to IBVPs defined after Eq. (10), although we focus here, for electron heat conduction, on the laser-imprint problem of direct-drive irradiation [12,14,15]. Note then, that for the present similarity flows, the fluid external boundary is held to be the critical density surface, i.e., the locus of zero density perturbation regardless of heat-flux modulations. Laser imprinting of flows I and II by a unit relative laser-intensity modulation has been investigated with this high accuracy numerical approach for extensive ranges in time and modulation wave number. Figure 2 illustrates the disparity—up to seven decades in amplitude for modulation wave numbers spanning four decades—in ablation-front distortion responses that may be captured by this approach. These responses [Fig. 2(b)] also evidence the significant reduction in imprint efficiency as the relative conduction zone size, $k_\perp l_{\rm con} (\equiv k_\perp L_{\rm con} t^\alpha)$, at which the intensity modulation starts to be applied is increased; a fact already established by laser-imprint simu-

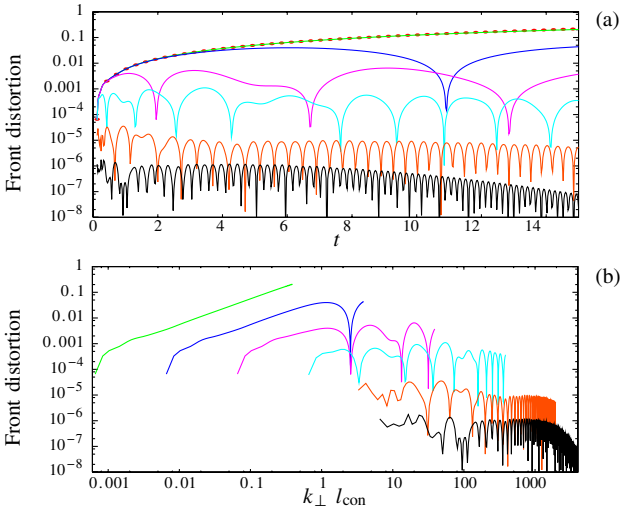

FIG. 2 (color online). Flow II of Table I. Dimensionless plots of the ablation-front distortions vs (a) time and (b) the relative distance $k_\perp l_{\rm con}$, for (top to bottom) wave numbers $k_\perp = 0$ [• in plot (a) only], 0.01, 0.1, 1, 10, 50, and 100.

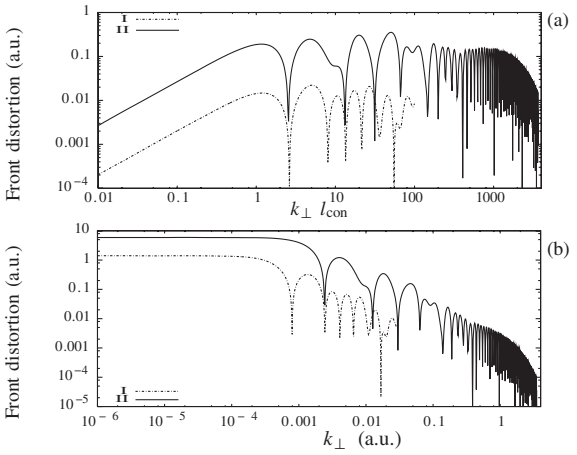

FIG. 3. Comparison between flows I and II of Table I. Plots, in arbitrary units (a.u.), of ablation-front distortion (a) responses vs the relative distance $k_\perp l_{con}$ for a particular modulation wavelength, and (b) spectra at shock breakout (the values for $k_\perp = 0$ being assigned to $k_\perp = 10^{-6}$).

lations and modeling [12,14,15]. The rough features of front distortion evolutions—the existence of a growth regime for $k_\perp l_{con} \ll 1$, and of a damped oscillatory regime for $k_\perp l_{con} \gg 1$—are recovered here. However, analyses of front distortions, η_{abl}, obtained for various wave numbers $k_\perp$, over the same range of the relative distance $k_\perp l_{con}$, and for each of the flows I and II [Fig. 3(a)] evidence significant differences with previous findings. Hence our results—valid for all $k_\perp l_{con}$, contrarily to the sharp boundary model of Ref. [14]—reveal the existence of three different regimes for the evolution of η_{abl}. For $k_\perp l_{con} \ll 1$, the distortion amplitude growth is algebraic, $\eta_{abl} \propto t^{4/3}$, and not linear [12,14,15], with the leading constant independent of $k_\perp$, and is due to the mean flow stretching effect on the continuous ablation layer profiles. In particular, mean flow and perturbation characteristic evolution times are identical, thus making irrelevant any stability analysis of this regime based on quasisteady mean flow arguments. The second regime, of modulated amplitude oscillations, follows for $1 \lesssim k_\perp l_{con} \lesssim 10^3$, the growth phase [Fig. 3(a)]. This regime, which has never been previously identified and could have important implications in experiments, sees the distortion amplitudes reaching their maximum—varying, as for constant irradiations [14,15], like $k_\perp^{-1}$—after a single [Fig. 3(a), curve I] or several phase reversals [Fig. 3(a), curve II], rather than at the end of the growth phase [14]. Such a behavior is consistent with the destabilizing influence of the mean flow stretching which is larger for flow II than for flow I. The third regime, of damped oscillations, only appears for very large values of $k_\perp l_{con}$ [Fig. 3(a), curve II for $k_\perp l_{con} \gtrsim 10^3$], the ablation layer characteristic length approaching then the modulation wavelength, with frequencies and damping factors becoming proportional, respectively, to $k_\perp t^{1/3}$ and $t^{4/3} \exp\{-\mathrm{cst} k_\perp t^{4/3}\}$, in contrast to the constant ($\propto k_\perp$) frequencies and $\exp\{-\mathrm{cst} k_\perp t\}$ dampings of Ref. [14]. Futhermore, maximum instability at $k_\perp = 0$ [Figs. 2(a) and 3(b)], a trend also noticed for constant irradiations [15], as well as a front distortion amplitude and oscillation period increase (Fig. 3) with a laser ramp pulse steepening $[\overline{\varphi}_x^{II}(0, t) > \overline{\varphi}_x^{I}(0, t)]$—in agreement with the mean flow stretching destabilizing effect—are demonstrated.

In summary, we have presented a fully—both physically and numerically—consistent approach to the linear stability of self-similar ablative flows and its application to the first analysis of laser imprinting based on a dynamic solution, revealing the determining effects of mean flow unsteadiness and ablation layer finite gradients.

We thank Dr. L. Hallo (CEA) and Professor R. Betti (Univ. of Rochester) for stimulating discussions, and Dr. X. Fortin (CEA) for sharing LMJ direct-drive data. F. A. acknowledges support from Professor R. Gatignol (Univ. of Paris VI) during his Ph.D.

*Previous address: CPhT, Ecole Polytechnique, 91128 Palaiseau, France.
†Electronic address: jean-marie.clarisse@cea.fr

[1] J. D. Lindl *et al.*, Phys. Plasmas **11**, 339 (2004).
[2] S. Bodner, Phys. Rev. Lett. **33**, 761 (1974); K. A. Brueckner and S. Jorna, Rev. Mod. Phys. **46**, 325 (1974); J. D. Lindl and W. C. Mead, Phys. Rev. Lett. **34**, 1273 (1975).
[3] H. J. Kull and S. I. Anisimov, Phys. Fluids **29**, 2067 (1986); H. J. Kull, Phys. Fluids B **1**, 170 (1989); V. V. Bychkov *et al.*, Sov. Phys. JETP **73**, 642 (1991); J. Sanz, Phys. Rev. Lett. **73**, 2700 (1994); J. Sanz, Phys. Rev. E **53**, 4026 (1996); R. Betti *et al.*, Phys. Plasmas **2**, 3844 (1995); V. N. Goncharov *et al.*, Phys. Plasmas **3**, 1402 (1996); A. R. Piriz *et al.*, Phys. Plasmas **4**, 1117 (1997).
[4] R. Marshak, Phys. Fluids **1**, 24 (1958).
[5] S. I. Anisimov, JETP Lett. **12**, 287 (1970).
[6] L. Brun *et al.*, in *Laser Interaction and Related Plasma Phenomena*, edited by H. J. Schwarz and H. Hora (Plenum, New York, 1977), Vol. 4B, p. 1059.
[7] A. Barrero and J. R. Sanmartin, Phys. Fluids **20**, 1155 (1977); J. R. Sanmartin and A. Barrero, Phys. Fluids **21**, 1957 (1978).
[8] Y. Saillard (unpublished).
[9] P. Reinicke and J. Meyer-ter-Vehn, Phys. Fluids A **3**, 1807 (1991).
[10] J. Sanz *et al.*, Phys. Fluids B **4**, 683 (1992).
[11] C. Boudesocque-Dubois, Ph.D. thesis, University Paris VI, 2000; in *ECLIM 2000*, edited by M. Kálal, K. Rohlena, M. Šiňor, Proceedings of SPIE Vol. 4424, p. 220 (2001).
[12] A. L. Velikovich *et al.*, Phys. Plasmas **5**, 1491 (1998).
[13] F. Abéguilé, Ph.D. thesis, University Paris VI, 2004.
[14] V. N. Goncharov, Phys. Rev. Lett. **82**, 2091 (1999); V. N. Goncharov *et al.*, Phys. Plasmas **7**, 2062 (2000).
[15] A. J. Schmitt *et al.*, Phys. Plasmas **8**, 2287 (2001).
[16] S. Gauthier *et al.*, Int. J. Pure Appl. Math. **24**, 553 (2005).
[17] H. Guillard *et al.*, J. Comput. Phys. **102**, 114 (1992); F. Renaud and S. Gauthier, J. Comput. Phys. **131**, 89 (1997).
[18] E. G. Gamaly *et al.*, Sov. Phys. JETP **52**, 230 (1980).
[19] C. Boudesocque-Dubois *et al.*, J. Comput. Phys. **184**, 592 (2003).